On Mooney and Mooney Stress Relaxation. II. A Nonlinear Viscoelastic Description: Experimental and Numerical Results

PAUL A. M. STEEMAN, JO H. M. PALMEN

DSM Research BV, P.O. Box 18, 6160 MD Geleen, The Netherlands

Received 9 September 1998; accepted 14 January 1999

ABSTRACT: It has been investigated whether the stress build-up and the stress relaxation involved in a Mooney test, with subsequent Mooney stress relaxation, can be described by nonlinear viscoelastic theory, more particularly the Wagner constitutive model. For this purpose, the viscoelastic behavior of three nonvulcanized EPDM materials, with similar Mooney viscosity but varying elasticity, has been studied. Relaxation time spectra were obtained from dynamic mechanical experiments, from which the step-strain stress-relaxation modulus was calculated. Stress build-up experiments were performed with a cone and plate system in order to obtain the so-called damping function (a measure for the deformation sensitivity) of the materials. Using these material functions, the Mooney test was successfully described with the Wagner constitutive model. Experimental and theoretical Mooney stress-relaxation rates are in close agreement. The predicted Mooney viscosity is up to 25% lower than the measured value. This may be due to nonideal conditions during the Mooney test, such as inhomogeneous heating and secondary flows, and to inaccuracy of the damping function. The model calculations confirm the strong experimental dependence of Mooney measurements on small variations in instrumental conditions such as geometry, rotation speed, and so forth. © 1999 John Wiley & Sons, Inc. J Appl Polym Sci 74: 1220–1233, 1999

Key words: rubber; EPDM; rheology; Mooney; viscosity; elasticity; stress relaxation; Wagner constitutive model

INTRODUCTION

The Mooney viscosity test (ASTM D 1646) is widely used for product specification and quality control of non-vulcanized rubbery materials. Additionally, Mooney stress relaxation (after the cessation of steady flow) was introduced[1,2] in order to provide additional information on the elasticity of the material. Standard instruments have been developed that allow for routine investigation, according to the rules of the norm, to determine the Mooney viscosity and the Mooney stress-relaxation rate (MSR). Because of the very large deformations applied during the Mooney test (typically several hundred shear units), the results are highly nonlinear viscoelastic. Therefore, the relation between Mooney results and linear viscoelastic material functions, such as the step-strain stress-relaxation modulus, well known to be a sensitive indicator for details of the molecular structure, is not straightforward.

Dynamic mechanical analysis, which gives direct access to the linear viscoelastic material functions, is widely used for rheological characterization of polymeric melts and rubbers. Harrell and Nakajima[3] introduced a modified Cole–Cole plot, plotting the loss modulus G'' versus the storage modulus G' (with varying frequency), in order

Correspondence to: P. Steeman.

Journal of Applied Polymer Science, Vol. 74, 1220–1233 (1999)
 CCC 0021-8995/99/051220-14

Table I Characteristics of the Samples from the Mooney Test and the Dynamic Mechanical Analysis at 125°C

Material	ML (1 + 4) Experimental	MSR Experimental	$\Delta\delta°$	ML Predicted from DMA with Cox–Merz
a	46.7	0.916	37.0	34.8
b	44.2	0.640	17.0	34.2
c	46.2	0.460	5.4	45.3

to emphasise the effects of broadening the molar mass distribution and of the presence of long-chain branching on the viscoelastic properties of nonvulcanized rubbers. Similarly, Booij[4] promoted the use of a so-called $\Delta\delta$-value, the difference between the phase angle δ at an angular frequency of 100 rad/s and at 0.1 rad/s, as an indicative parameter for the presence of long-chain branching (LCB) in nonvulcanized EPDM rubbers. Low $\Delta\delta$-values indicate the presence of a significant level of LCB.

Experimental practice suggests some correlation between the Mooney stress-relaxation slope and the dynamic mechanical properties,[5] for example, the $\Delta\delta$-value. Vennemann and Lüpfert[2] analyzed the Mooney stress-relaxation curves with Fourier analysis, thus extracting the loss tangent (tan δ). However, because the Mooney test is highly nonlinear, whereas the dynamic test is performed in the linear viscoelastic range, relations between Mooney results and the small-strain dynamic mechanical properties are not self-evident. These results triggered a theoretical investigation of the Mooney viscosity and the Mooney stress-relaxation test.[6] It was shown that Mooney stress relaxation, in general, strongly differs from stress relaxation at small strain. For example, if the Mooney test were a linear viscoelastic test, hardly any stress relaxation would occur during the time interval studied. Thus, it can be concluded that the Mooney test is highly *nonlinear,* and can be correctly described only with nonlinear theories. For this purpose, the Wagner constitutive model[7] or, more generally, the K-BKZ constitutive equation[7] (as described by White[8]), may be used. The analytical treatment in the earlier study[6] has shown the potentials of this approach. However, in view of the simplifications used in the analytical treatment, as well as of the nonuniform deformation field in the Mooney test cell (disc type rotor), a numerical treatment is necessary to obtain a complete description.

For this purpose, the calculation scheme employed by Nakajima and Harrell[9] and by White and Tokita[10] can be used. Assuming a power-law viscosity function for the rubber, they integrated the stresses over the whole flow field in the Mooney test cell in order to calculate the torque during steady shear flow. Dove and coworkers[11] used a modified Maxwell element, replacing the damper by a power-law liquid, in order to describe also the stress-relaxation part. In this study, a full nonlinear viscoelastic description is applied, which allows for the calculation of both the stress build-up and the stress relaxation.

EXPERIMENTAL

Three nonvulcanized sample EPDM materials (samples *a*, *b,* and *c*) with similar Mooney viscosity, but significantly different elasticity, were selected (Table I).

Dynamic mechanical experiments in shear with angular frequencies between 10^{-4} and 10^{2} rad/s were performed at 125°C with a Rheometric Scientific DSR200 controlled-*stress* rheometer, equipped with a 25-mm diameter *parallel plate* geometry.

Stress build-up and relaxation experiments in shear were performed with a Rheometric Scientific controlled-*strain* rheometer RMS800, equipped with a *cone-and-plate* geometry with a cone angle of 0.2 radians ($\cong$11.5 degrees). Experiments were performed at shear rates of 0.01 and 0.04 rad/s with a total shear time of 1000–3600 sec, after which the stress relaxation was recorded. These shear rates are 1 to 2 decades lower than the rate applied during a Mooney test. Stress build-up, even at these low shear rates, caused distortion of the sample geometry at high shear; therefore, the data at the longest times or highest shear are less reliable. Higher shear rates would result in even more distortion of the samples, whereas normal forces would

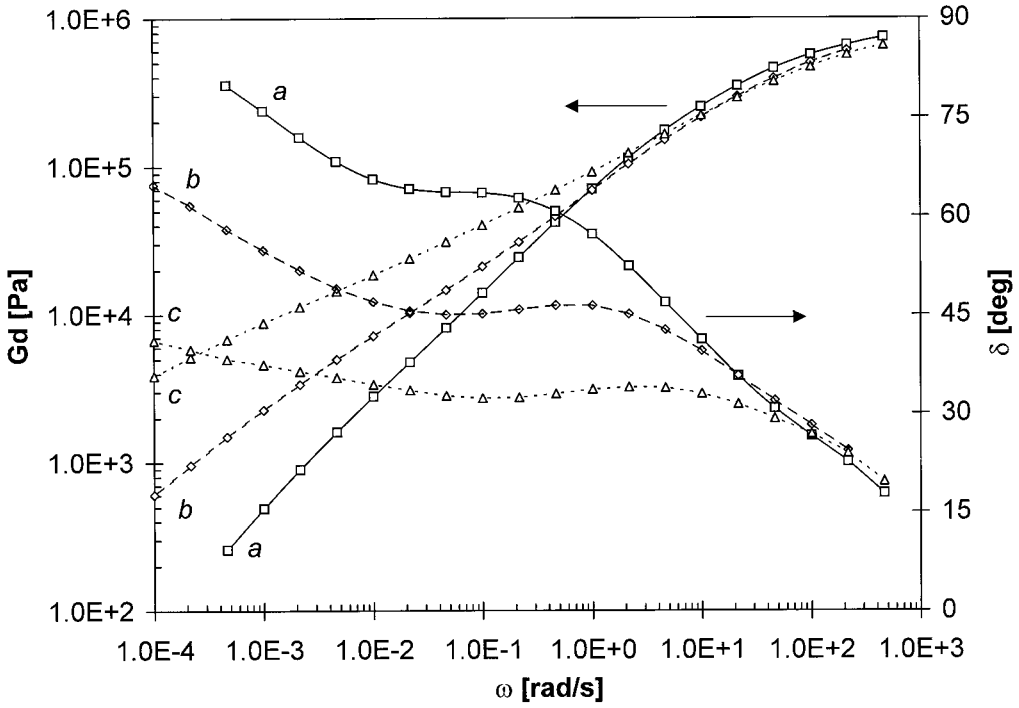

Figure 1 The dynamic mechanical properties of the three EPDM materials.

become too high for the instrument. Therefore, higher shear rates could not be used. The samples of material *c* (highest elasticity) repeatedly failed during the stress build-up experiments. As a consequence, no stress-relaxation curves could be obtained for this material.

Mooney measurements were performed with a Monsanto MV2000 Mooney viscometer. The Mooney viscosity ML (1 + 4) was measured at 125°C, according to the ASTM D1646 standard. The Mooney viscosity was calculated as the torque after 1 min preheating and 4 min shearing (2 rev/min) with the standard large rotor. The Mooney stress relaxation rate (MSR) was determined from the slope of the double logarithmic decay of the torque M between 1.2 and 6 s after rotor stop (i.e., the exponent α in $M(t) = K^*t^{-\alpha}$). Details of the sample chamber geometry can be obtained from the ASTM standard. Because of the disc-shaped rotor, a nonuniform deformation field is applied to the sample. At the rotor center the deformation rate is zero, whereas at the rotor edge the deformation rate between the rotor and the upper and lower plates amounts to about 1.57 s^{-1}. After a rotation time of 240 s, this results in a total deformation of about 380 shear units, which is far beyond the linear viscoelastic range.

Table I lists the sample characteristics as determined with the Mooney test and with dynamic mechanical analysis at 125°C.

THEORY

As in Struik's earlier study in this series,[6] we attempt to describe the Mooney stress build-up and relaxation with the Wagner constitutive model for the nonlinear viscoelastic behavior of polymer melts,[7] which is an extension of the linear viscoelastic theory incorporating the deformation sensitivity of the material via a so-called damping function.

Linear viscoelastic theory (Boltzmann integral) states that the shear stress σ at time t is given by the integration over the history ξ ($-\infty \leq \xi \leq t$) of the deformation $[\gamma(t) - \gamma(\xi)]$ multiplied with the memory function $m(t - \xi)$:

$$\sigma(t) = \int_{-\infty}^{t} m(t - \xi)[\gamma(t) - \gamma(\xi)]d\xi \qquad (1)$$

in which

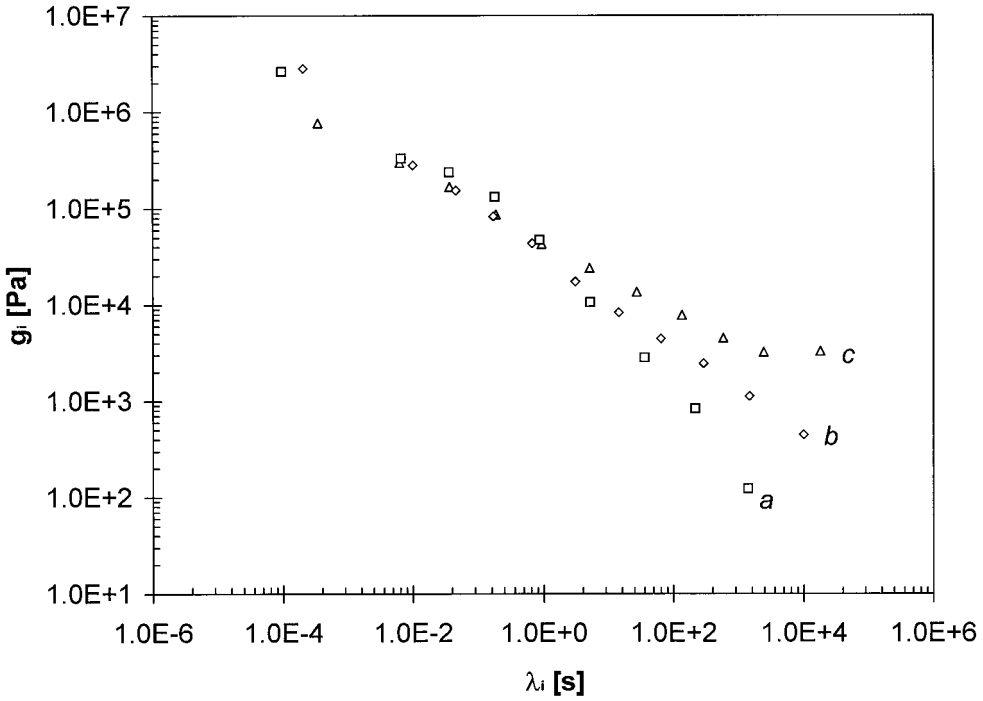

Figure 2 The relaxation time spectra of the three EPDM materials.

$$m(t) = -\frac{\partial G(t)}{\partial t} \tag{2}$$

The *memory function* $m(t)$ can be determined from the time derivative of the *step-strain stress relaxation modulus* $G(t)$. Alternatively, an oscillatory experiment can be performed, since the dynamic moduli can be converted into the stress-relaxation modulus.[12] The dynamic results may also be converted into the relaxation time spectrum, from which both the memory function and the stress-relaxation modulus can be derived. For reasons of computational ease the latter approach was adopted. Calculations were performed with the program IRIS™ (Baumgärtel and Winter), specially designed for this purpose.

Wagner introduced a modification of the linear theory in order to take the deformation sensitivity (nonlinear behavior) of the material into account. For this purpose, the separability of strain and time effects was incorporated. A so-called *damping function* $h(\gamma)$, describing the deformation sensitivity of the material, was introduced into the kernel of the integral:

$$\sigma(t) = \int_{-\infty}^{t} m(t-\xi) \cdot |h(\gamma(t) - \gamma(\xi))| \cdot [\gamma(t) - \gamma(\xi)] d\xi \tag{3}$$

For small strains, $h(\gamma) = 1$; $h(\gamma)$ decreases with increasing strain γ, indicating that large strains cause relatively smaller stresses. Wagner has shown[13] that stress build-up experiments are well suited for determining the damping function $h(\gamma)$, provided that the linear viscoelastic behavior of the material is known. Wagner proposed to extract the damping function from the stress build-up curve ($\gamma(t) = \dot{\gamma}t$ with $\dot{\gamma} = const$) using[13]:

$$h(\gamma) = \frac{\dfrac{\sigma(t)}{G(t)} - \displaystyle\int_0^t \sigma(t') \frac{m(t')}{G^2(t')} dt'}{\dot{\gamma}t} \tag{4}$$

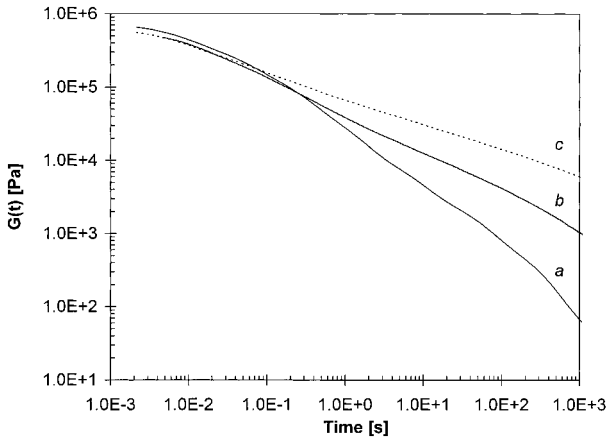

Figure 3 The calculated stress-relaxation curves.

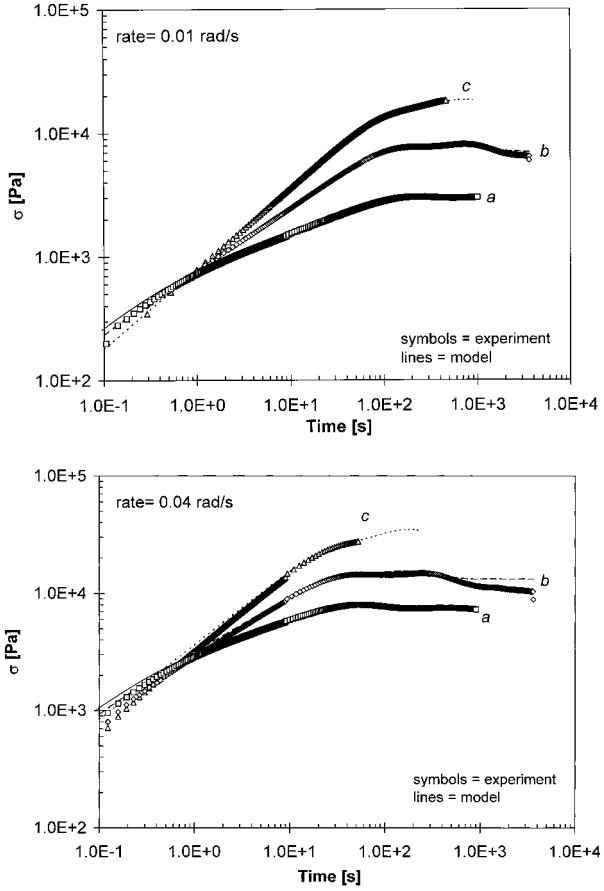

Figure 4 a. The stress build-up during steady shear with a rate of 0.01 s^{-1}. 4b. The stress build-up during steady shear with a rate of 0.04 s^{-1}.

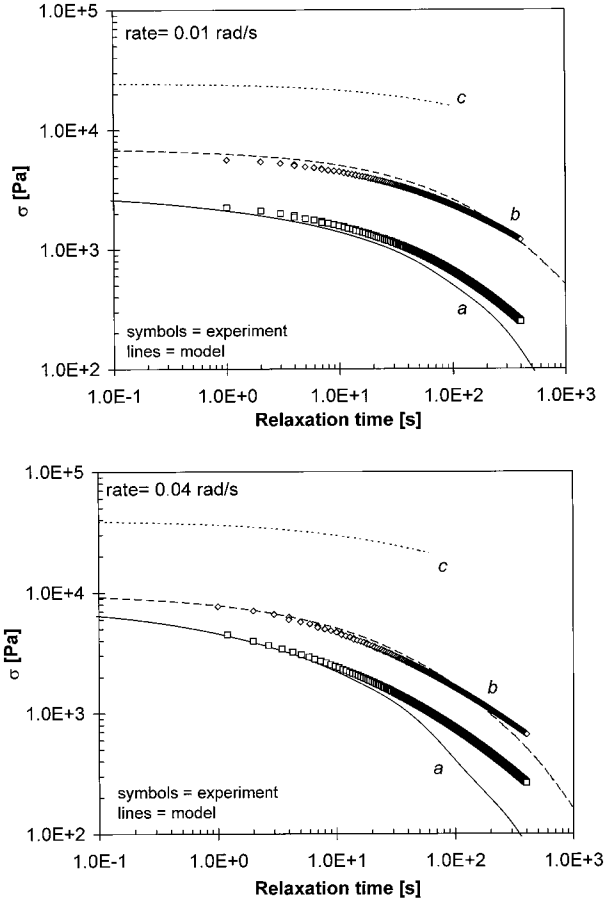

Figure 5 a. The stress relaxation after steady shear with a rate of 0.01 s^{-1}. 5b. The stress relaxation after steady shear with a rate of 0.04 s^{-1}.

in which $\sigma(t)$ is the measured shear stress at time t, whereas $m(t)$ and $G(t)$ are the memory function and the (step-strain) stress-relaxation modulus, respectively, as determined with the linear viscoelastic (dynamic or step-strain) experiments.

RESULTS

The Linear Viscoelastic Response

Figure 1 shows the results of the dynamic mechanical measurements on the three EPDM materials. The dynamic modulus $G_d = |G^*|$ is plotted along the left axis, whereas the phase angle δ is plotted along the right axis, both as a function of angular frequency ω.

The materials show a clear distinction in the elasticity at angular frequencies below 10 rad/s, which is attributed to a varying content of long-chain branching.[4] The $\Delta\delta$-value, the difference

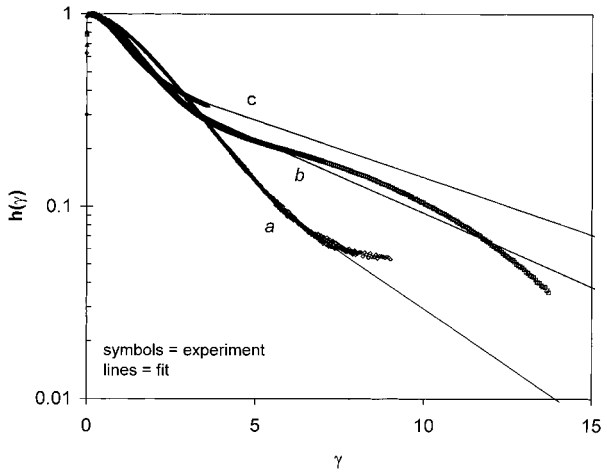

Figure 6 The damping functions in shear of the three EPDM materials.

Table II Damping Function Parameters for the Three Materials

Material	f	n_1	n_2
a	0.546	0.134	0.274
b	0.459	0.368	0.177
c	0.440	0.512	0.137

between the phase angle at 0.1 rad/s and at 100 rad/s is listed in Table I for the three materials. Sample a, which is the least elastic, shows a shoulder in the phase angle at intermediate frequencies and an increase to 90 degrees at the lowest frequencies. This indicates that the material behaves nearly Newtonian on a time scale of 10^4 s or more. By contrast, sample c, which is the most elastic, shows a nearly frequency independent and low value of the phase angle. On a time scale of 10^4 s, no tendency toward Newtonian behavior is observed. Meanwhile, its low-frequency dynamic modulus is much higher than that of the other two materials. The large difference in elasticity of the materials in the low-frequency range clearly illustrates the sensitivity of dynamic measurements to long-chain branching as was shown earlier by Harrell and Nakajima[3] and Booij.[4]

Experience has shown that the dynamic viscosity η_d at $\omega = 1$ rad/s can be used as an estimate of the Mooney viscosity: ML (1 + 4) 125°C $\approx \eta_d(\omega = 1$ rad/s, $T = 125$°C)/2000[Pa*s]. This approximation is based on the Cox–Merz rule $\eta_d(\omega) \approx \eta(\dot{\gamma} = \omega)$. A similar equation has been proposed by Ninomiya and colleagues.[14] The Mooney viscosity as calculated from the dynamic experiments (DMA) has been included in Table I.

Figure 2 shows the *discrete* relaxation time spectra as calculated from the dynamic results with the program IRIS™.

The program is constructed such that the minimum number of relaxation times are selected to describe the dynamic data accurately. For the EPDM materials studied, 10 to 12 relaxation times are sufficient. Figure 2 shows the intensities g_i [Pa] (y-axis) of the various relaxation times λ_i [s] (x-axis). From this figure it can be clearly recognized that increasing elasticity is associated with higher intensities (g_i) at longer relaxation times (λ_i). For sample c, the spectrum is probably truncated at long times because the measurement time was too short for accurate determination of the slowest relaxation processes.

Using these relaxation time spectra both the stress relaxation modulus $G(t)$ and the memory function $m(t)$ of the materials can be calculated with

$$G(t) = \sum_i g_i e^{-t/\lambda_i} \tag{5}$$

and

$$m(t) = -\frac{\partial G(t)}{\partial t} = \sum_i \frac{g_i}{\lambda_i} e^{-t/\lambda_i} \tag{6}$$

Figure 3 shows the stress relaxation modulus $G(t)$ as a function of time for the three materials. For $t' > 0.1$ s, the curves resemble a power law curve $G(t) \sim t^{-n}$ as used by Struik for his calculations in the earlier study.[6]

The Nonlinear Viscoelastic Response

Figures 4a and b show the shear stress versus time for the three materials during the stress build-up in the RMS800. Figures 5a and b show the stress relaxation experiments. Shear rates were 0.01 and 0.04 rad/s. The symbols in Figures 4 and 5 are the experimental results, whereas the

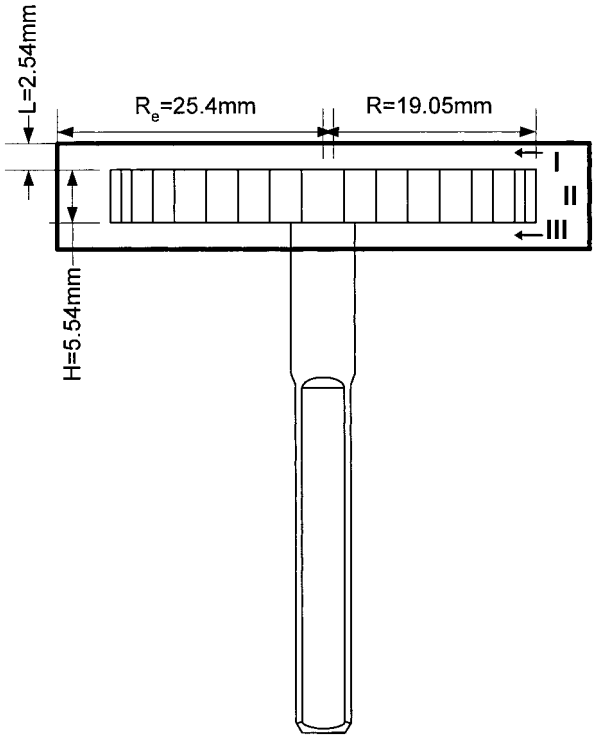

Figure 7 Schematic view of the Mooney test cell.

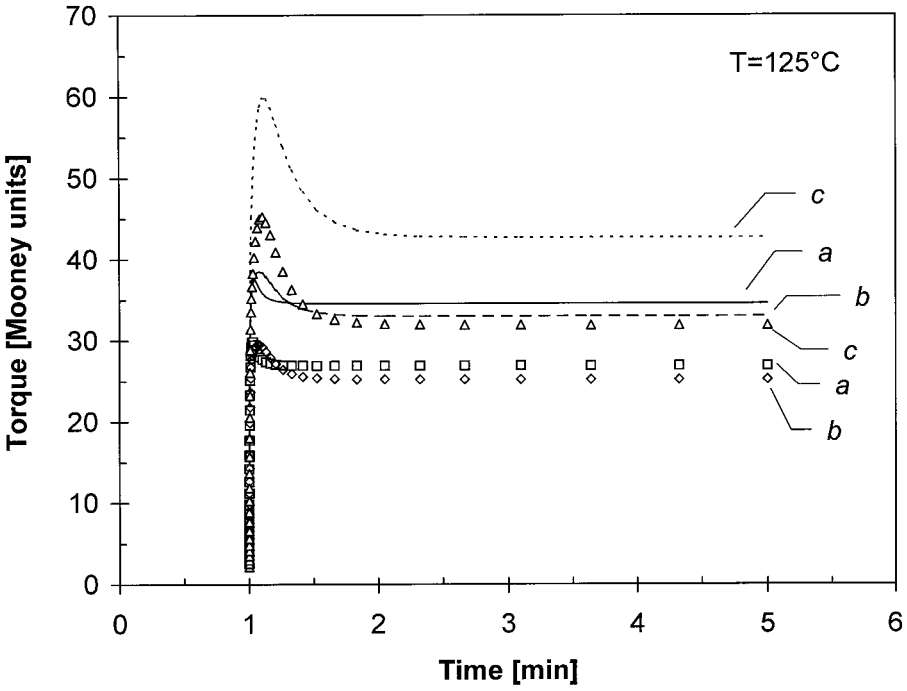

Figure 8 Calculated Mooney stress build-up curves. The symbols show the stress due to the upper and lower rotor surfaces and the lines, the total stress.

lines are the results of constitutive modeling as is discussed later.

Figures 4a and b show for all materials in the beginning a sharp increase of the shear stress with time. After 30 to 100 s the shear stress levels off and reaches an equilibrium value. At higher shear rates the equilibrium is obtained after shorter shear times, but at comparable total strain. During the stress build-up experiments a total shear of 10–40 is applied, which is in the nonlinear viscoelastic range, though less far than in the Mooney test. However, since the equilibrium stress is obtained at a strain of about 2–3, extrapolation to higher strains (100–400) seems possible without introducing large errors. Figure 6 depicts the damping functions for the three materials as a function of the deformation γ.

Sample *c*, the most elastic material, is slightly more deformation sensitive at small strains than the materials *a* and *b*. However, at higher strains, sample *c* is clearly the least deformation sensitive. It appears that EPDM materials become less deformation sensitive with increasing LCB content. This phenomenon is well known from literature for polyethylenes.[15]

The damping function in shear is often modeled with an exponential function of the total shear γ with one or more terms. We obtained a good description when two terms are used, with the first quadratic in the deformation γ.

$$h(\gamma) = f \cdot e^{-n_1\gamma^2} + (1 - f) \cdot e^{-n_2\gamma} \qquad (7)$$

The values of f, n_1, and n_2 giving the best description are listed in Table II. This table demonstrates the slightly larger deformation sensitivity of the materials with higher LCB content at smaller deformations (increasing n_1-coefficient) and, more significantly, the lower deformation sensitivity at larger strain (decreasing n_2-coefficient and increasing weight f).

Using the damping function and the relaxation time spectrum, the stress build-up and relaxation were calculated with the Wagner constitutive eq. (3). The curves in Figures 4 (build-up) and 5 show the results of these calculations. An accurate description of the build-up is obtained for all samples. The stress relaxation is overestimated at long times, mainly for sample *a,* at the highest shear rate. This might indicate that the actual damping is less than the damping function predicts or that the relaxation time spectrum is truncated. Note that the stress relaxes only slightly

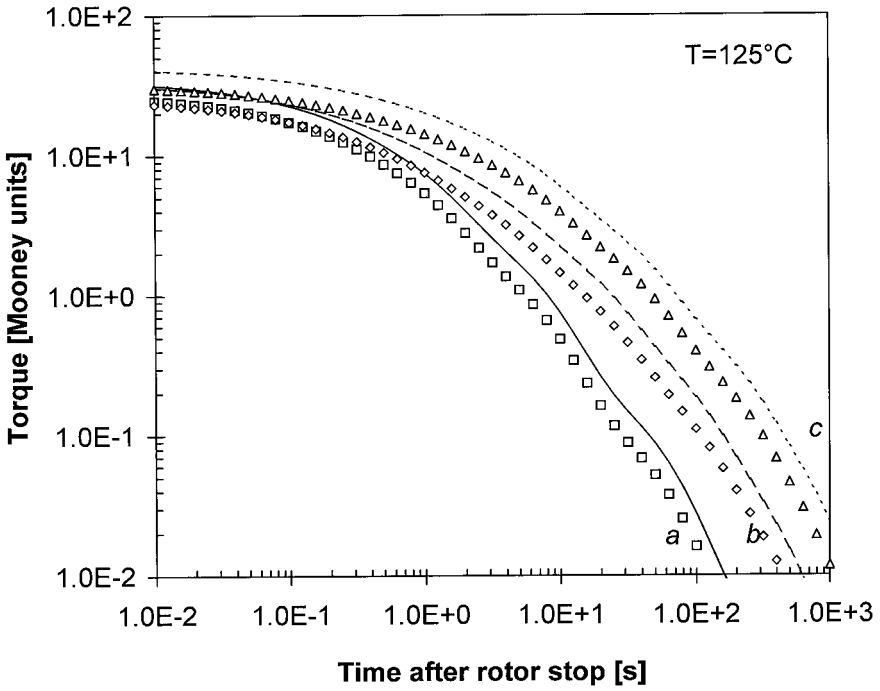

Figure 9 Calculated Mooney stress relaxation curves. The symbols show the stress due to the upper and lower rotor surfaces and the lines, the total stress.

during the first 10 s after rotor stop (determination of the MSR), similar to the predictions from linear viscoelastic theory by Struik,[6] but in contrast to the experimental observations of the Mooney stress relaxation.

Modeling of the Mooney Test

In Figure 7, the Mooney test cell with the large rotor is depicted, which according to the ASTM standard D1646 can be used for the Mooney viscosity and relaxation measurements.

Usually, the rotor and the walls of the cell are serrated in order to minimize slip effects. The rotor is rotated with 2 revolutions per minute. Standard measurement temperature for EPDM rubber is 125°C.

In view of the construction of the cell, three deformation regions I, II, and III (see Fig. 7) have to be considered:

1. Between the rotor and the upper plate of the cell (region I)
2. Between the rotor edge and the sidewall (region II)
3. Between the rotor and the lower plate of the cell and the rotor shaft (region III)

Neglecting the influence of the rotor shaft, regions I and III are identical. Because of the disc-shaped rotor, a deformation gradient ranging from zero shear at the rotor center to maximum shear at the rotor edge (radius = R) is present in these regions. In region II, between rotor edge ($r = R$) and the sidewalls (r

Table III Mooney, Relaxation Slope, and δ-Values for the Three EPDM Materials

Material	ML (1 + 4) Calculated Wagner	MSR Calculated Wagner	δ ° (ω = 0.1 rad/s)	δ ° (ω = 100 rad/s)	Slope, $G(t)$ (t = 10 s)
a	34.6	0.951	63.5	26.5	0.77
b	33.0	0.627	45.1	28.2	0.46
c	42.7	0.467	32.3	26.9	0.32

$= R_e$), the deformation gradient along the rotor surface is zero. Following Leblanc,[16] the total torque M on the rotor can be calculated from:

$$M = 2 \cdot \int_0^R 2\pi r(r\sigma_{\theta z})dr + 2\pi Rh[R(\sigma_{r\theta})_R] \quad (8)$$

in which $\sigma_{\theta z}$ and $\sigma_{r\theta}$ are the shear stresses on the surfaces (at a given radial position) and on the edge of the rotor, respectively. The shear stresses can be calculated with the Wagner constitutive eq. (3), making use of the damping functions and the memory functions as derived from the stress build-up experiments (RMS800) and the dynamic experiments (DSR200), respectively. The shear rates in the various regions are:

$$\dot{\gamma}(r) = \Omega r/L \quad \text{with} \quad 0 < r < R \quad (9)$$

at the rotor surface (region I/III) and:

$$\dot{\gamma}(R) = 2\Omega R^2/(R_e^2 - R^2) \quad (10)$$

at the rotor edge (region II), in which Ω is the rotation speed (rad/s) of the rotor. In the case of 2 revolutions per minute (Ω = 0.21 rad/s), the deformation rate at the rotor surfaces ranges from 0 to 1.57 s^{-1}, whereas the rate at the rotor edge amounts to about 0.54 s^{-1}.

The total torque on the rotor, calculated with eq. (8), can be easily converted into Mooney values using the definition according to the ASTM standard that *a torque of 0.083 N m^{-1} equals one Mooney unit*.

Figures 8 and 9 show the results of the calculations for the stress build-up and relaxation experiments on the three materials, where the torque is given in Mooney units.

The curves give the total torque, whereas the symbols show the results for regions I and III, thus without the rotor edge. The figures show that 20 to 30% of the torque is due to the rotor edge, that is, it is not allowed to ignore the edges. The calculated ML (1 + 4) 125°C values are listed in Table III.

DISCUSSION

The Mooney Viscosity

Figure 10 shows the experimental Mooney viscometer curves. Several conclusions can be drawn from Figures 8, 9, and 10 and Table III.

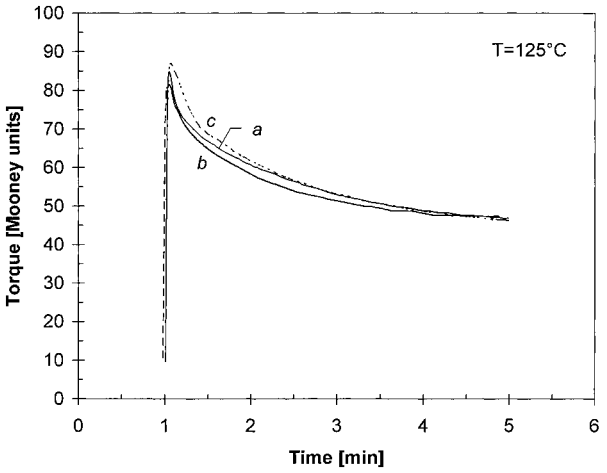

Figure 10. The experimental Mooney stress build-up curves.

- Qualitatively, the calculated results resemble the actual Mooney curves measured with the Mooney viscometer (Fig.10). During the first minute of stress build-up a pronounced maximum in the torque is predicted, similar to the stress peak during the Mooney test, after which a steady value is obtained. The model calculations predict, in accordance with theoretical predictions,[6] that the stress peak occurs within 15 s after rotor start
- The model calculations indicate, again in accordance with theoretical predictions,[6] that the maximum is weak (<110% of steady value) for sample *a* (the least elastic material), stronger (≈120%) for sample *b,* and most significant (>130%) for sample *c* (the most elastic material). By contrast, the actual Mooney results show for all samples a comparable and much larger magnitude (≈190%) of the maximal torque.
- The model calculations predict that the steady state is obtained within 30 s after rotor start, whereas the actual Mooney test results show that the decrease of the torque in time continues for more than 4 min.
- Comparison of Table I and Table III shows that the predicted and the measured steady-state values for the Mooney viscosity differ significantly. Except for sample *c*, the predicted Mooney viscosities are up to 25% smaller than the measured values. By contrast, the predictions are in close agreement with the results from the dynamic tests (Table I). The Cox–Merz relation seems to hold

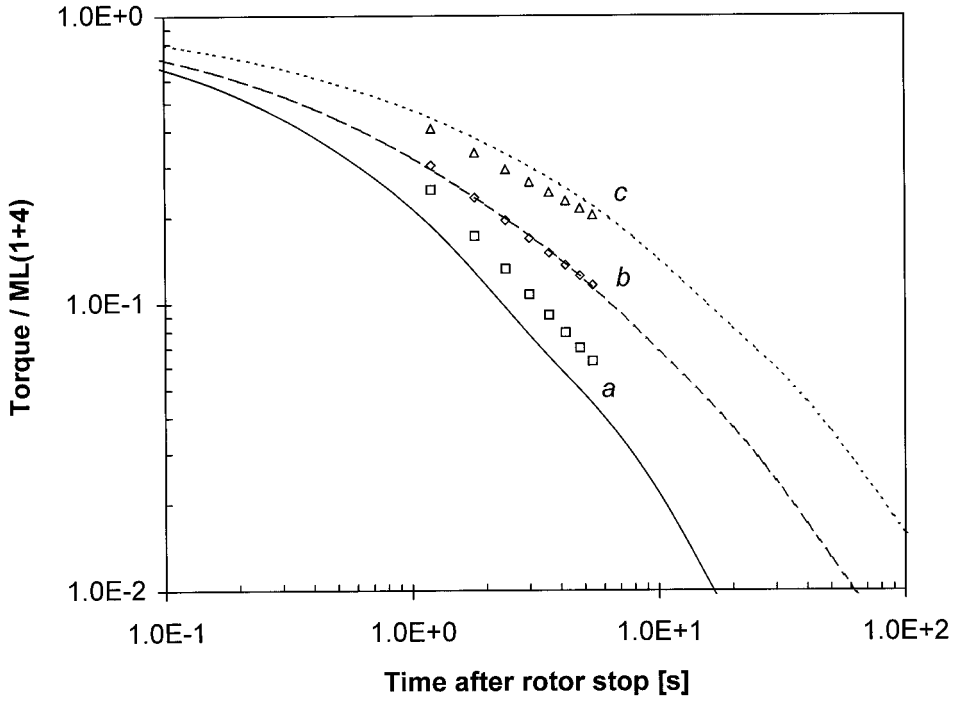

Figure 11 The experimental Mooney stress relaxation (symbols) and the calculated curves (lines).

and predicts the steady-state viscosities in agreement with the Wagner model calculations.

Several effects may account for the differences between calculations and experiments:

- Inaccuracy or strain-rate dependence of the (extrapolated) damping functions (e.g., the deformation sensitivity is overestimated).
- Truncated relaxation time spectra, underestimating the longest relaxation times.
- Incomplete description of the sample chamber geometry; for example, the corners connecting regions I and II and regions II and III are not taken into account. Therefore, the calculated stress level may be too low.
- Experimental artifacts during the Mooney test such as:

1. Nonuniform heating and insufficient thermal equilibration in the Mooney test cell (some evidence for this is presented in the appendix).
2. Settling effects (after filling) in the Mooney viscometer lasting more than 1 min, which may broaden the torque maximum and cause the torque to decay continuously.
3. Secondary flow in the Mooney viscometer, induced by the generated normal forces, which causes the torque to increase.
4. Effects due to the serrated plates and cell walls. In the calculations a flat rotor and flat surfaces were assumed.
5. Sample constriction and failure in the Mooney viscometer due to the large deformations, similar to the effects that occurred in the RMS800 rheometer during the stress build-up measurements (e.g., sample *c*), causing the experimental Mooney to be too low.

In view of these possible sources of errors, especially the experimental artifacts, no further attempts were made to improve the accuracy of the description.

The Mooney Stress Relaxation

Figure 11 shows the experimental (symbols) and the calculated (lines) Mooney stress relaxation of the three materials. The torque was normalized to the steady-state value ML (1 + 4) 125°C at rotor stop.

Figure 11 shows that the slopes of the experimental and the calculated stress relaxation curves are in good agreement. The differences in the absolute values between the experimental and the calculated torques, though normalized, are probably due to the possible experimental artifacts as discussed earlier.

The Mooney stress-relaxation rate (MSR) was determined from these curves by performing a linear regression analysis on the logarithm of the stress versus the logarithm of time. Figure 11 shows that the power law approximation used for the calculation of the MSR is valid over a limited time interval, in accordance with the theoretical predictions by Struik.[6] The experimental and calculated MSR values are listed in Table III. A very good agreement, within 4%, between calculated and experimental MSR is obtained. This indicates that the stress-relaxation part of the Mooney test, during which no flow occurs in the test cell, is accurately described with the Wagner model.

Finally, Table III also contains the slope of the stress relaxation modulus $G(t)$ versus time at t = 10 s after the application of a step-strain (calculated from the relaxation time spectra) and the experimental phase angles δ obtained from the dynamic measurements at ω = 0.1 rad/s and at ω = 100 rad/s.

The $\Delta\delta$-parameter, $\Delta\delta = \delta(0.1 \text{ rad/s}) - \delta(100 \text{ rad/s})$, was introduced[4] as an indicator for the presence of long-chain branching (LCB) in EPDM materials. The phase angle at ω = 100 rad/s mainly depends on the molar mass (Mooney level) of the material, whereas the phase angle at ω = 0.1 rad/s is also strongly influenced by the elastic effects due to LCB.[4] Therefore, the difference of these angles was found to be a good, molar-mass independent (i.e., Mooney independent) indicator for the presence of LCB.

No simple relation between $\Delta\delta$ and the slope of the stress-relaxation modulus versus time is to be expected. However, in agreement with earlier theoretical findings by Booij and Thoone[17] the theoretical relation between the phase angle δ [deg] at ω = 0.1 rad/s and the slope of the stress relaxation modulus at $t = 1/\omega$ = 10 s is experimentally found:

$$\text{Theoretical: } \frac{-\partial \log G(t)}{\partial \log t} \approx \left.\frac{\partial \log G(\omega)}{\partial \log \omega}\right|_{(\omega=1/t)} \approx \delta°/90 \quad (11)$$

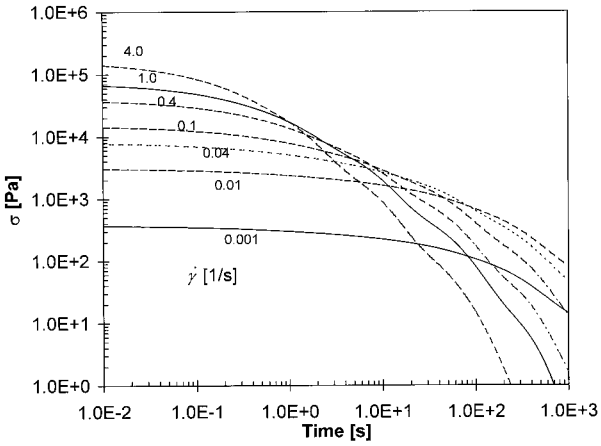

Figure 12 Stress relaxation curves at various shear rates.

$$\text{Experimental: } \frac{-\partial \log G(t)}{\partial \log t} \approx [0.011 \pm 0.001] \cdot \delta(0.1\text{rad/s}) \quad (12)$$

For the Mooney stress-relaxation rate (MSR) such theoretical relations are neither known, nor expected.[6] In this study, we empirically found that

$$\text{Experimental: MSR} \approx (0.0140 \pm 0.0001) \cdot \delta(0.1 \text{ rad/s}) \quad (13)$$

In contrast to (small) step-strain stress relaxation, the stress relaxation after the cessation of steady shear flow depends strongly on the experimental conditions; for example, the deformation rate during the preceding stress build-up measurement has a very large effect. At very low rates (linear viscoelastic regime) only minor stress relaxation is to be expected during the first 10 s after the cessation of flow. This is illustrated in Figure 12, which shows the predicted stress-relaxation curves of material *a* after shearing with various rates. With increasing shear rate, the slope of the stress-relaxation curve increases sharply. This confirms the strong experimental dependence of Mooney viscosity and Mooney stress relaxation on small variations in instrumental conditions such as the geometry, the rotation speed of the rotor, and so forth. Therefore, these should be accurately controlled in order to obtain reliable and reproducible results. Dynamic measurements and step-strain stress-relaxation measurements in the linear viscoelastic regime are less critical in this sense.

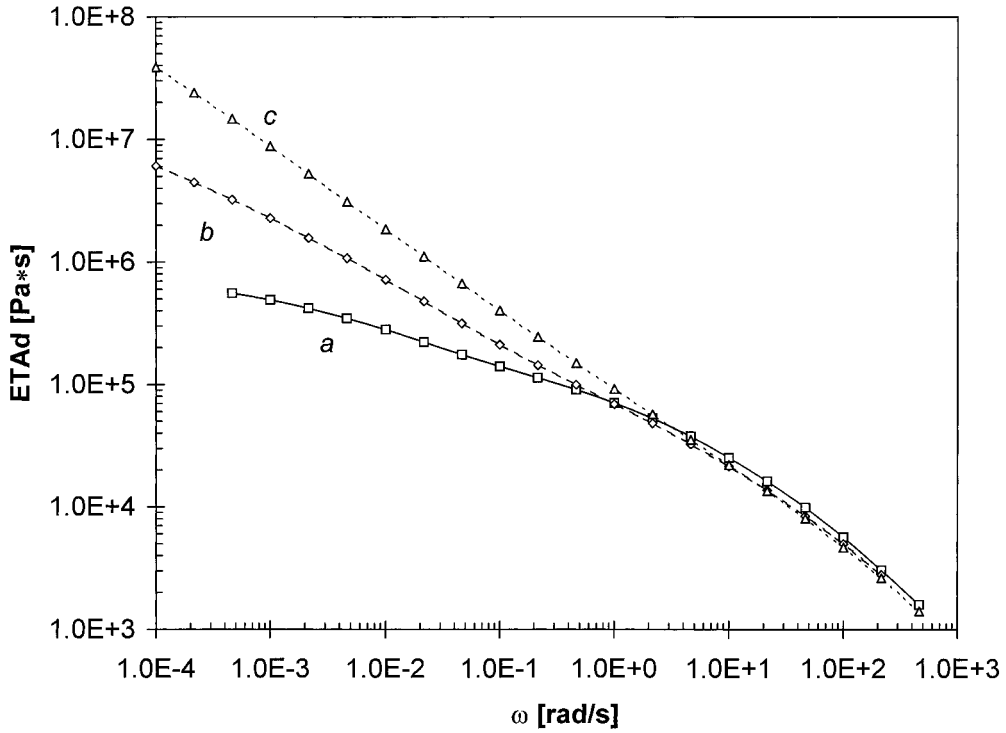

Figure 13 The dynamic viscosity of the three EPDM materials versus the angular frequency.

It is concluded that the measured MSR is not a linear viscoelastic property, but due to a combined effect of both linear (spectrum) and nonlinear (damping function) viscoelastic properties of the material. Therefore, no simple theoretical relation between the MSR and linear viscoelastic properties (such as the slope of the stress-relaxation modulus or the $\Delta\delta$), valid for all types of nonvulcanized rubber materials, is to be expected. The Mooney stress-relaxation curve differs strongly from the stress relaxation at low strain.

It should be noted that the Mooney viscosity is a single-point parameter, which in this case, for example, displays only minor variations among the three types. This could suggest a comparable processibility of the materials. However, differences in elasticity, as found from the Mooney stress relaxation MSR, indicate that this is not the case. From dynamic mechanical analysis, the curve of the dynamic viscosity η_d versus angular frequency ω can be obtained (Fig. 13). Assuming the validity of the Cox–Merz rule (the dynamic viscosity at angular frequency ω equals the steady-state viscosity at $\dot{\gamma} = \omega$), Figure 13 shows the complete flow curves of the materials.

This figure clearly displays the significantly different flow behavior of the three materials at lower shear rates. These differences are of particular importance for those processing and material properties, which are related to the low or zero shear viscosity. For material *a,* the zero-shear viscosity can be extracted, which is not the case for the other two materials. Although the Mooney viscosities of the materials are about equal, the zero shear viscosities appear to be significantly different. For material *c,* it is probably several decades higher than for material *a*. By contrast, at high shear rates occurring during high-speed processing, material *c* has the lowest viscosity and the processibility order seems to be reversed. Thus, the combination of Mooney viscosity and Mooney stress-relaxation rate offers more insight into the processibility of the materials. The results presented here show the added value of dynamic mechanical analysis over the Mooney test, as was also concluded by Breemhaar and coworkers[18] on the basis of more empirical evidence.

CONCLUSIONS

- Mooney stress build-up and stress relaxation can be described with nonlinear viscoelastic theory.

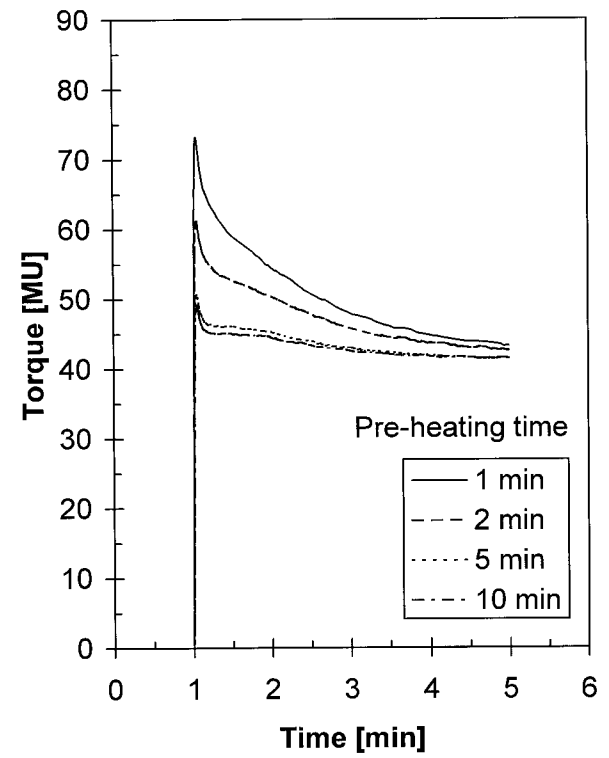

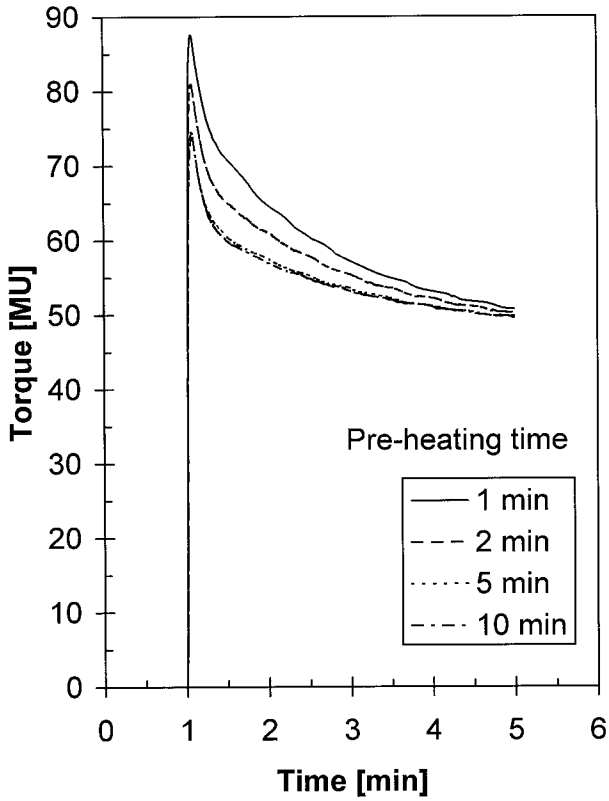

Figure 14 a. Experimental Mooney stress build-up curves for sample *a* after various thermal equilibration times. For clarity, all curves were shifted to a fictive starting time of 1 min. 14b. Experimental Mooney stress build-up curves for sample *c* after various thermal equilibration times. For clarity, all curves were shifted to a fictive starting time of 1 min.

- The Wagner integral constitutive equation is suitable for this purpose.
- Relaxation time spectra and damping functions, the input for the Wagner model, can be extracted from oscillatory measurements and from stress build-up and relaxation experiments at low shear rates with a cone-and-plate geometry, respectively.
- The Mooney viscosity calculated with the Wagner model, taking the sample cell geometry into account, agrees to within 25% with the measured values. Experimental artifacts during the Mooney test probably account for a major part of these deviations.
- The Mooney stress-relaxation rate calculated with the Wagner model, again taking the sample cell geometry into account, agrees within 4% with the experimental values.
- Both the Mooney viscosity and the Mooney stress-relaxation rate are highly nonlinear viscoelastic properties.
- The theoretical relationship between the phase angle from oscillatory measurements and the slope of the small-strain stress-relaxation modulus as a function of time is experimentally confirmed.
- For the MSR, no theoretical relationship with the phase angle exists. The experimentally observed correlation with the phase angle at $\omega = 0.1$ rad/s is the result of a complex interplay between the relaxation time spectrum and the damping function, and holds only for the given experimental conditions and the studied materials.
- MSR and ML are single-point measurements, which each on its own reveal only limited information about the complex rheological behavior of EPDM. Their combination is much more powerful. The benefit of dynamic mechanical analysis is reconfirmed.

APPENDIX

The Effect of Thermal Equilibration on the Mooney Curves

In order to obtain adequate thermal equilibrium before starting the Mooney measurements, the

standards commonly prescribe 1-min equilibration time after inserting the sample in the viscometer cell. In our laboratory, it was investigated whether this time interval is sufficient (unpublished results). The effect of thermal equilibration time on the Mooney curves was investigated by varying the equilibration time between 1 and 10 min. Figure 14a and b show the results for sample *a* and *c*. It appears that thermal equilibrium is not obtained during the standard 1-min equilibration time. Due to nonuniform heating a much larger stress peak occurs, especially for the least-elastic sample *a* (Fig. 14a). The curves after at least 4-min equilibration are more nearly similar to the calculated curves than the data obtained after 1-min equilibration. Nonuniform heating probably accounts for the major part of the differences between theoretical calculations using the Wagner constitutive model and the experimental Mooney results.

REFERENCES

1. Koopmann, R. K.; Kramer, R. K. J Test Eval 1984, 12(6), 407.
2. Vennemann, N.; Lüpfert, S. Kautsch Gummi Kunstst 1991, 44(3), 270.
3. Harrell, E. R.; Nakajima, N. J Appl Polym Sci 1984, 29, 995.
4. Booij, H. C. Kautsch Gummi Kunstst 1991, 44(2), 128.
5. Meijers, P. W. L. J.; Maag, L. R.; Beelen, H. J. H.; van de Ven, P. M. Presented at the meeting of the Süd-Deutsches Kunststoff-Zentrum, Neuentwicklungen bei Rohstoffen für die Kautschukindustrie, Advances in EPDM Production Technology: Controlled Long Chain Branching as the key to improved product performance and consistency; Wurzburg; October 1997.
6. Struik, L. C. E. J Appl Polym Sci 74, 5, 1207.
7. Larson, R. G. Constitutive equations for polymer melts and solutions; Butterworths: New York, 1988.
8. White, J. L. Rubber Chem.Technol 1977, 50, 163.
9. Nakajima, N.; Harrell, E. R. Rubber Chem Technol 1979, 52(1), 9.
10. White, J. L.; Tokita, N. J Appl Polym Sci 1974, 9, 1929.
11. Dove, R. A.; Turner, D. M.; Martin, T. Rubbercon '77, The International Rubber Conference, 1977; p 29.1.
12. Ferry, J. D. Viscoelastic properties of polymers; Wiley: New York, 1967.
13. Wagner, M. H. J Non-Newtonian Fluid Mech 1978, 4, 39–55.
14. Ninomiya, K.; Kusamizu, S.; Maekawa, E.; Yasuda, G. Prog Polym Sci (Japan), Imoto, M., Ed.; Vol. 1; Kodanska LTD: Tokyo, 1971; p 377.
15. Booij, H. C.; Palmen, J. H. M.; Leblans, P. J. R. in Interrelations between linear viscoelastic and nonlinear rheological quantities in transient shear flow of polymer melts, Proceedings of IX Intl. Congress on Rheology, Mexico, 1984; p 367.
16. Leblanc, J. Rheologie des elastomeres et mise en oeuvre des polymeres; Artel Publishers: Namur, 1996.
17. Booij, H. C.; Thoone, G. P. J .M. Rheol Acta 1982, 21, 15.
18. Breemhaar, W.; Koopmann, R.; Markert, J.; Noordermeer, J. Kautsch Gummi Kunstst 1993, 46, 957.